Clays and Clay Minerals, Vol. 38, No. 6, 573–583, 1990.

POLARIZED SINGLE-CRYSTAL FOURIER-TRANSFORM INFRARED MICROSCOPY OF OURAY DICKITE AND KEOKUK KAOLINITE

C. T. JOHNSTON,[1] S. F. AGNEW,[2] AND D. L. BISH[3]

[1] Department of Soil Science, 2169 McCarty Hall, University of Florida
Gainesville, Florida 32611

[2] INC-4 Mail Stop C346
[3] EES-1 Mail Stop D469
Los Alamos National Laboratory, Los Alamos, New Mexico 87545

Abstract—Single-crystal Fourier-transform infrared (FTIR) spectra of Keokuk kaolinite and Ouray dickite were obtained with an FTIR microscope. Although numerous IR, FTIR, and Raman spectra of polycrystalline kaolinite and dickite can be found in the literature, the present data represent the first reported single-crystal vibrational spectra for these clay minerals. The orientation of the crystallographic axes of dickite was determined using a cross-polarizing optical microscope fitted with an 550-nm optical retardation plate. Assignment of the inner hydroxyl group OH_1 to the 3623-cm^{-1} band was confirmed, and the angle of this OH group to the *b*-axis was determined to be 47° based upon the measured dichroic ratio. The 3702–3710-cm^{-1} absorption feature appeared to consist of two closely spaced bands having slightly different polarization behavior. The inner-surface hydroxyl group OH_3 was assigned to the absorption bands at 3710 cm^{-1}. The calculated angle of the OH_3 groups to the *b*-axis was found to be 22°, which agrees well with the angles determined by X-ray powder diffraction and neutron diffraction. The remaining hydroxyl groups, OH_2 and OH_4, were assigned to the 3656 cm^{-1} band; the angle of the OH_2 and OH_4 groups to the *b*-axis was measured at 45°. The polarization behavior of the OH-deformation bands of dickite at 911, 937, and 952 cm^{-1} was found to be similar to that observed in the OH-stretching region. Single-crystal FTIR spectra of Keokuk kaolinite showed that rotation of the electric vector around the *c*/z axis in the *ab* plane of kaolinite resulted in a behavior distinct from that of dickite. The OH-stretching bands of kaolinite were found to be considerably more polarized than the corresponding bands of dickite. This is related directly to the fact that dickite possesses a glide plane (space group *Cc*) compared with kaolinite, which does not (space group C_1).

Key words—Crystal structure, Dickite, Fourier-transform infrared microscopy, Hydroxyl orientation, Kaolinite, Single crystal.

INTRODUCTION

The OH groups of kaolin-group minerals have attracted considerable attention as sensitive indicators of structural disorder and of change resulting from the presence of guest species in the interlayer region (Barrios *et al.*, 1977; Johnston *et al.*, 1984; Brindley *et al.*, 1986; Raupach *et al.*, 1987; Bookin *et al.*, 1989; Prost *et al.*, 1989). In particular, the OH-stretching and -deformation vibrational modes have been shown to correlate strongly with the degree of disorder (Barrios *et al.*, 1977; Prost *et al.*, 1989), the Hinckley index (Brindley *et al.*, 1986), and changes in interlayer bonding (Wieckowski and Wiewiora, 1976; Giese, 1982; Johnston and Stone, 1990). Controversy remains, however, regarding the assignment of these bands to the four distinct structural OH groups present in kaolinite and dickite (Giese, 1988). Although the 3620-cm^{-1} infrared (IR) band has been assigned unambiguously to the inner OH group (Ledoux and White, 1964; Rouxhet *et al.*, 1977), no general consensus exists regarding the assignment of the IR-active 3652-, 3668-, or 3695-cm^{-1} bands for kaolinite.

Assignment of the OH-stretching bands of kaolinite and dickite has been further complicated by the observation of an additional Raman-active ν(O–H) band at 3682 cm^{-1} for kaolinite (Wiewiora *et al.*, 1979; Johnston *et al.*, 1985; Michaelian, 1986). Similar features have been reported in the low-temperature IR spectrum of dickite, in which five distinct bands occur (Prost *et al.*, 1989). Group theory predicts a maximum of four ν(O–H) bands for both dickite and kaolinite based upon the *Cc* and C_1 space groups, respectively. The presence of at least five bands for the two polymorphs indicates that a lower symmetry space group must apply for the complete structure (i.e., upon inclusion of the hydrogen atoms). Suitch and Young (1983) and, more recently, Young and Hewat (1988) reported that the appropriate space group for kaolinite was *P*1 based upon Rietveld structure refinements of X-ray powder diffraction and neutron diffraction data. A primitive Bravais lattice would account for the greater-than-predicted number of ν(O–H) bands; however, these refinements of the non-hydrogen framework and the suggested *P*1 space group have been criticized recently (Brindley *et al.*, 1986; Thompson and Withers, 1987; Bish and Von Dreele, 1989; Thompson *et al.*, 1989).

Attempts to locate the positions of the hydrogen atoms in kaolinite and dickite using various structural methods have not resulted in an unambiguous descrip-

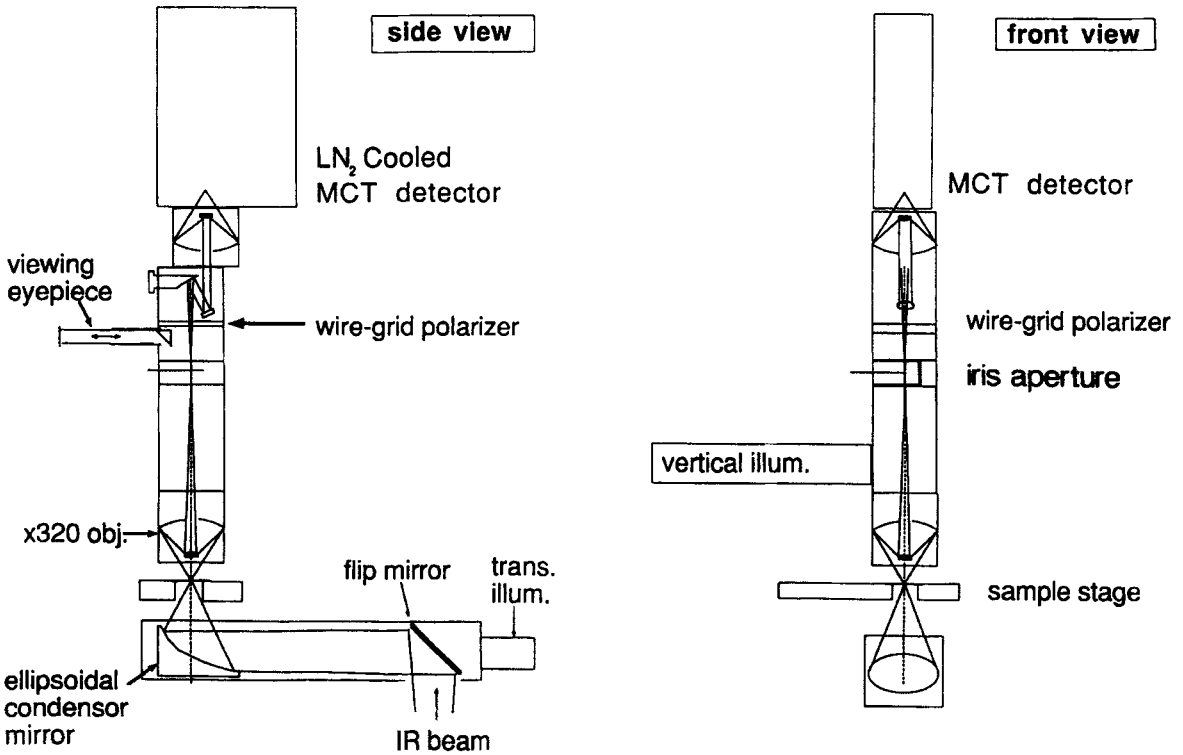

Figure 1. Schematic of the Digilab IR100 microsampling accessory.

tion of the OH groups (Adams and Hewat, 1981; Giese, 1982; Adams, 1983; Suitch and Young, 1983; Sen Gupta *et al.*, 1984; Joswig and Drits, 1986; Young and Hewat, 1988). The available structural data for the OH groups are presented in Tables 1 and 2 for kaolinite and dickite, respectively. As these data indicate, there is relatively poor agreement regarding the bond length and overall position of the hydrogen atoms, despite the fact that structures have been refined for both polymorphs using neutron diffraction data. For example, OH bond lengths in kaolinite range from 0.829 to 1.47 Å, with equal uncertainties present in the measured angle of the OH bond out of the 001 plane and in the angle between the projection of the OH bond onto the 001 plane with the *b*-axis. Polarized infrared studies of oriented deposits of kaolinite have provided indirect evidence of the OH orientations by indicating that the transition moment for the 3695-cm^{-1} band is nearly perpendicular to the 001 plane, whereas the 3620-, 3652-, and 3668-cm^{-1} bands have little pleochroism upon tilting the oriented deposit (Rouxhet *et al.*, 1977; Prost *et al.*, 1987). This observation is not consistent with the current consensus that all three of the inner-surface OH groups of kaolinite are oriented normal to the 001 plane (Giese, 1988). Surprisingly, little effort has been put forth to reconcile the suggested hydrogen positions obtained from neutron, electron, and X-ray powder diffraction studies with the observed IR and Raman spectra of kaolin polymorphs.

The primary objectives of this study were to obtain polarized Fourier-transform infrared (FTIR) spectra of single-crystal specimens of Ouray dickite and Keokuk kaolinite and to determine the orientations of the hydroxyl groups. The measured dichroic ratio for a particular band relates directly to the direction of the transition moment for that particular vibrational mode (Turrell, 1972). Thus, the observed dichroic ratios for the ν(O–H) bands of dickite and kaolinite should provide new insight about the orientation of the structural OH groups, similar to earlier polarized IR studies of the OH groups in micas (Vedder and McDonald, 1963) for which large single crystals are available. The reported vibrational spectra for Ouray dickite and Keokuk kaolinite (Brindley *et al.*, 1986) agree well with the large body of spectra obtained for polycrystalline samples which have been reported for kaolinite and dickite (Wada, 1967; Farmer, 1974). Thus, the polarization behavior of these specimen samples should relate directly to the smaller particle sizes of kaolinite and dickite samples that are typically found in soils and sedimentary deposits. In addition, the single-crystal kaolinite and dickite spectra obtained here should serve as a prototypic application of FTIR microscopy to characterize clay minerals and related soil constituents.

https://doi.org/10.1346/CCMN.1990.0380602 Published online by Cambridge University Press

Table 1. Summary of structural parameters for the OH groups of dickite.

Reference	Label	r(OH) (Å)	Angle of OH with *b*-axis	Angle of OH with (001) plane	Distance O–H···O (Å)	Angle <OH···O (deg)	Distance O···O (Å)	Direction cosines (direction angles = A, B, C) cos A	cos B	cos C	Al–O bond lengths (Å) Al1–OH	Al2–OH	Avg Al–O	Al(1)–O–Al(2) bond angle Al–O–Al
Inner hydroxyl OH1														
Joswig and Drits (1986)	H1	0.745	25°	0°				−0.424	−0.906	0.004	1.915	1.913	1.914	100.3°
								−0.424	0.906	0.004				
Sen Gupta *et al.* (1984)	H1	0.891	31°	22°				−0.482	−0.790	−0.380				
								−0.482	0.790	−0.380				
Adams and Hewat (1981)	H1	1.126	31°	−18°				−0.489	−0.813	−0.315				
								−0.489	0.813	−0.315				
Giese and Datta (1973)	H1	0.971	31°	15°				−0.492	−0.833	0.253				
								−0.492	0.833	0.253				
This study			47°											
Inner-surface OH2														
Joswig and Drits (1986)	H2	0.787	61°	76°	2.154	173°	2.937	0.208	−0.113	0.972	1.844	1.854	1.849	107.5°
								0.208	0.113	0.972				
Sen Gupta *et al.* (1984)	H2	0.715	70°	75°	2.223	177°	2.936	0.243	−0.086	0.966				
								0.243	0.086	0.966				
Adams and Hewat (1981)	H2	1.148	9°	63°	1.972	139°	2.937	0.071	−0.451	0.890				
								0.071	0.451	0.890				
Giese and Datta (1973)	H2	0.97	36°	75°	1.995	163°	2.937	0.153	−0.212	0.965				
								0.153	0.212	0.965				
This study			45°											
Inner-surface OH3														
Joswig and Drits (1986)	H3	0.859	11°	53°	2.36	149°	3.127	0.111	0.590	0.800	1.85	1.858	1.854	104.8°
								0.111	−0.590	0.800				
Sen Gupta *et al.* (1984)	H3	0.789	25°	56°	2.426	148°	3.125	0.238	0.511	0.826				
								0.238	−0.511	0.826				
Adams and Hewat (1981)	H3	1.249	22°	66°	1.946	156°	3.127	0.152	0.370	0.917				
								0.152	−0.370	0.917				
Giese and Datta (1973)	H3	0.973	5°	68°	2.163	171°	3.127	−0.034	0.374	0.927				
								−0.034	−0.374	0.927				
This study			22°											
Inner-surface OH4														
Joswig and Drits (1986)	H4	0.809	63°	69°	2.153	172°	2.956	−0.324	−0.168	0.931	1.848	1.849	1.849	107.7°
								−0.324	0.168	0.931				
Sen Gupta *et al.* (1984)	H4	0.914	62°	66°	2.051	169°	2.953	−0.358	−0.194	0.913				
								−0.358	0.194	0.913				
Adams and Hewat (1981)	H4	1.118	88°	60°	1.931	151°	2.956	−0.501	−0.018	0.865				
								−0.501	−0.018	0.865				
Giese and Datta (1973)	H4	0.969	80°	70°	2.005	167°	2.956	−0.337	−0.057	0.940				
								−0.337	0.057	0.940				
This study			45°											

Table 2. Summary of structural parameters for the OH groups of kaolinite.

Reference	Label	r(OH) (Å)	Angle of OH with *b*-axis	Angle of OH with (001) plane	Distance O–H···O (Å)	Angle <OH···O (deg)	Distance O···O (Å)	Direction cosines (direction angles = A, B, C)		
								cos A	cos B	cos C
Inner hydroxyl										
Young and Hewat (1988)	OH1	1.082	32°	−12°				0.524	0.827	0.204
Young and Hewat (1988)	OH5	0.99	31°	22°				0.481	0.794	−0.372
Adams (1983)	O(6)H6	0.87	40°	−36°				0.531	0.614	−0.584
Suitch and Young (1983)	H(1)–H(1)	0.85	24°	22°				0.382	0.842	0.380
Suitch and Young (1983)	H(5)–H(5)	1.15	42°	−10°				0.656	0.736	−0.168
Giese (1982) (Zvyagin structure)	H(6)	0.97	32°	14°				0.511	0.824	0.245
Giese (1982) (Brindley structure)	H(6)	0.96		15°						
Inner-surface OH1										
Young and Hewat (1988)	H(7)	1.041	84°	75°	1.986	173°	3.022	−0.259	0.026	0.965
Young and Hewat (1988)	H(3)	1.098	48°	48°	2.037	136°	2.927	−0.494	0.446	0.746
Adams (1983)	H(1)	0.924	77°	69°	2.043	169°	2.954	−0.342	0.078	0.937
Suitch and Young (1983)	H(7)	1.26	43°	76°	1.9	162°	3.125	−0.163	0.176	0.971
Suitch and Young (1983)	H(3)	0.927	41°	52°	2.231	142°	3.017	−0.402	0.468	0.787
Giese (1982) (Zvyagin structure)	H(1)	0.971	82°	76°	1.932	173°	2.898	−0.244	0.037	0.969
Giese (1982) (Brindley structure)	H(1)	0.974		70°						
Inner-surface OH2										
Young and Hewat (1988)	H(2)	1.042	78°	62°	1.949	153°	2.915	0.460	0.098	0.883
Young and Hewat (1988)	H(6)	0.955	69°	74°	2.298	158°	3.205	−0.259	0.026	0.965
Adams (1983)	H(2)	1.105	51°	69°	1.951	148°	2.943	0.305	−0.247	0.920
Suitch and Young (1983)	H(2)	1.476	62°	56°	1.941	144°	3.255	0.493	0.265	0.829
Suitch and Young (1983)	H(6)	0.855	38°	64°	2.373	137°	3.055	0.274	−0.352	0.895
Giese (1982) (Zvyagin structure)	H(2)	0.968	36°	78°	1.95	163°	2.89	0.120	−0.165	0.979
Giese (1982) (Brindley structure)	H(3)	0.974		72°						
Inner-surface OH3										
Young and Hewat (1988)	H(4)	0.908	79°	66°	1.986	143°	2.766	−0.404	−0.081	0.911
Young and Hewat (1988)	H(8)	1.049	8°	48°	2.089	145°	3.012	−0.098	−0.655	0.741
Adams (1983)	H(3)	1.033	48°	61°	2.166	146°	3.077	−0.361	−0.330	0.872
Suitch and Young (1983)	H(4)	1.115	45°	59°	2.248	141°	2.937	−0.366	−0.371	0.853
Suitch and Young (1983)	H(8)	0.829	32°	50°	1.991	145°	2.972	−0.342	−0.542	0.768
Giese (1982) (Zvyagin structure)	H(3)	0.974	29°	12°	2.361	136°	3.138	−0.478	−0.855	0.202
Giese (1982) (Brindley structure)	H(3)	0.974		61°						

MATERIALS AND METHODS

A highly crystalline dickite sample was studied from Red Mountain, Ouray, Colorado (obtained from G. W. Brindley). X-ray powder diffraction (XRD) was used to verify the identity of the dickite specimen. Orientation of the crystallographic axes was determined using a polarizing microscope fitted with a 550-nm quartz retardation plate. Relatively large (30–50 μm), pseudo-hexagonal, flake-like crystals of dickite were abundant. The Keokuk kaolinite sample was obtained from W. D. Keller and has been described previously (Keller, 1977). This is the same material used by Suitch and Young (1983), Young and Hewat (1988), and Bish and Von Dreele (1989) in studies of the kaolinite structure. The largest of the pseudo-hexagonal kaolinite crystals present was 5 to 10 μm across the 001 face. The Ouray dickite and Keokuk kaolinite samples were used as received, without further purification.

Single-crystal IR spectra were obtained on a Digilab FTS-40 FTIR spectrometer equipped with Digilab's IR100 microsampling accessory. The IR microscope was modified to incorporate a rotatable wire-grid polarizer about 2.5 cm above the iris aperture, as shown in Figure 1. The Digilab microscope incorporates a 90° elliptical mirror condensor and a 320× Cassegrain objective, which is mounted on a turret with a 40× viewing objective. The sample image is transferred to the iris aperture and can be viewed with visible light by means of an insertable viewing port, or the IR light can be relayed through the polarizer, recollimated by means of a 35° paraboloidal mirror, and imaged onto an MCT liquid N_2-cooled detector with another Cassegrain element. A liquid N_2-cooled narrow-band mercury-cadmium telluride detector was used to provide optimal response in the OH-stretch region. Spectra were collected using 2.0-cm^{-1} resolution, and 4096 to 8192 spectra were co-added with a triangular apodization function used in the Fourier transform.

Polarized spectra were obtained by positioning a selected crystal within the iris aperture and rotating the polarizer. The orientation of the crystallographic *a*- and *b*-axes was determined by observing the same sample under crossed polarizers with an optical microscope fitted with a 550-nm quartz retardation plate. As the diagram shown in Figure 2 illustrates, the *b*-axis of dickite is perpendicular to one side of the pseudo-hexagon, whereas the *a*-axis is parallel to this side (Kerr, 1977). The orientation of the crystallographic axes of kaolinite could not be determined, due to the smaller size of the Keokuk kaolinite crystals and interferences resulting from twinning.

A non-linear, least-squares band-analysis program was written to decompose the absorption spectra into individual spectral components. The fitting function allowed the Lorentzian-to-Gaussian character for a particular band to vary between 0 and 1. A linear baseline correction was applied to all of the data sets. The output from the program included the fitted position, full-width at half maximum (FWHM), integrated intensity, fractional Lorentzian character, and fraction of the total area occupied for each band. Typically, three to four bands (four adjustable parameters per band) were fitted at a time with a linear baseline correction for a total of 14 to 18 adjustable parameters.

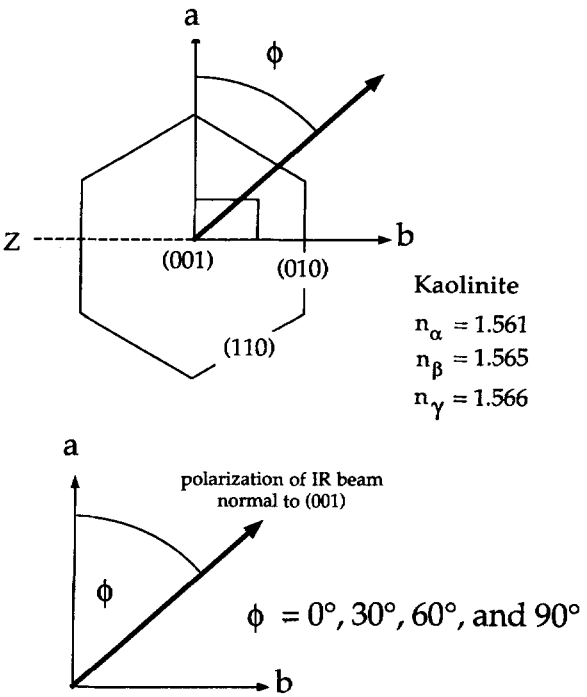

Figure 2. Optical orientation of crystallographic axes of idealized hexagonal-shaped crystal of dickite or kaolinite.

RESULTS

Dickite

Polarized single-crystal transmission FTIR spectra of Ouray dickite are shown in Figures 3a and 3b for the ν(O–H) region. Unambiguous assignment of the *a*- and *b*-crystallographic axes of dickite was determined using a polarizing optical microscope fitted with a 550-nm quartz retardation plate. Polarized single-crystal FTIR spectra were then obtained for a dickite crystal of known orientation. Figure 3a presents the FTIR spectra with no y-offset and the absolute intensity scale shown on the y-axis; the same data are shown in Figure 3b with polarization of the electric vector defined by the angle between the electric vector and the *a*-axis. The IR beam was at normal incidence upon the (001) face of the dickite particle, and the polarization of the electric vector of the incident beam was rotated around the c′/z axis (c′ is defined as normal to the (001) plane which deviates by 6.7° from the crystallographic *c*-axis).

https://doi.org/10.1346/CCMN.1990.0380602 Published online by Cambridge University Press

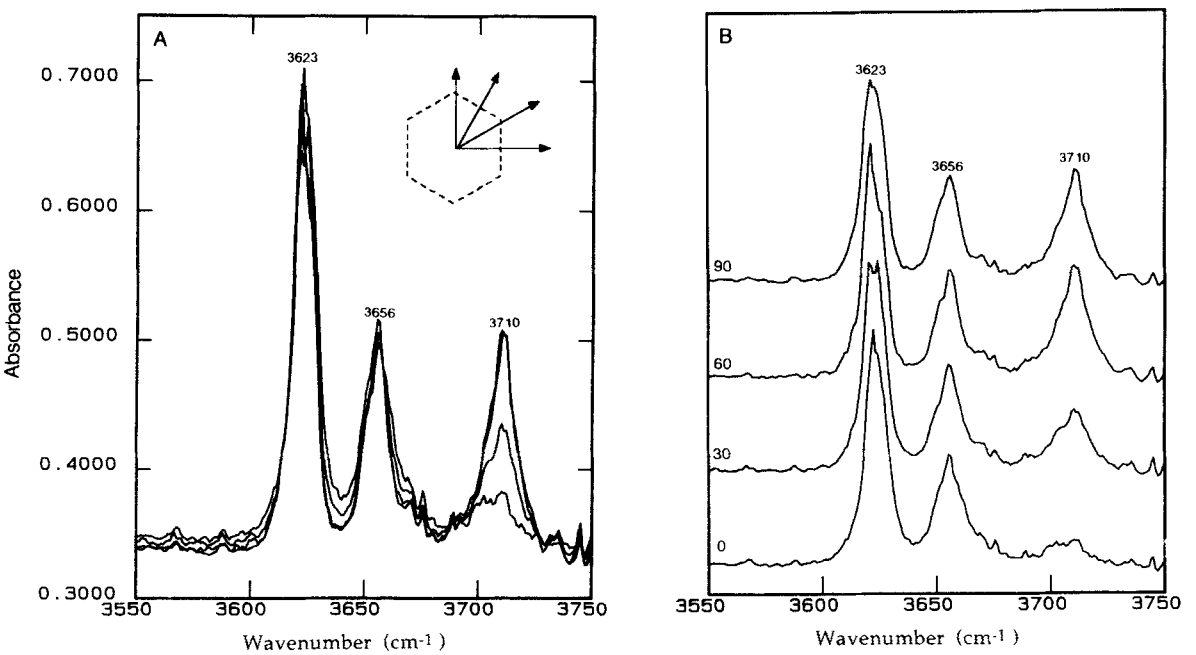

Figure 3. Polarized single-crystal Fourier-transform infrared spectra of Ouray dickite in the 3550–3750-cm^{-1} region. (a) Stack plot showing spectra with no y-offset with absorbance scale shown on left. (b) Same spectra in which listed polarization angles correspond to angle between electric vector of the transmitted infrared beam and crystallographic *a*-axis of the dickite crystal.

The observed ν(O–H) bands at 3623, 3656, and 3710 cm^{-1} are in good agreement with published spectra for dickite (Farmer, 1974; Prost, 1984; Brindley *et al.*, 1986; Prost *et al.*, 1987, 1989). Although numerous IR, FTIR, and Raman spectra have been reported for polycrystalline dickite and kaolinite materials (Farmer, 1974; Brindley *et al.*, 1986; Prost *et al.*, 1989), as far as the present authors are aware these spectra (Figures 3a and 3b) and the accompanying kaolinite spectra (Figures 6a and 6b) represent the first reported single-crystal vibrational spectra for kaolinite or dickite.

Polarized FTIR spectra of a dickite crystal were analyzed using a non-linear, least-squares band-analysis program. The results of the non-linear, least-squares band analysis in the OH-stretching region are presented in Table 3. If the polarization of the electric vector was parallel to the *b*-axis (top spectrum labeled 90°) the 3710-cm^{-1} band had maximum integrated intensity. Upon rotation of the electric vector towards the *a*-axis, the intensity of this band was reduced significantly. In contrast to the 3710-cm^{-1} band, the integrated intensity of the 3623-cm^{-1} band reached a maximum if the electric vector was polarized parallel to the *a*-axis (bottom spectrum labeled 0°). Plots of the integrated intensity of the 3623- and 3710-cm^{-1} bands vs. the polarization of the electric vector in the 001 plane (angles measured from the *a*-axis) are presented in Figure 4. The position, bandwidth, and intensity of the 3656-cm^{-1} band were not influenced significantly by rotation of the electric vector around the c'-axis. The 3623-cm^{-1} band also appeared to have a some fine structure, which changed upon rotation. FTIR spectra of a thinner dickite crystal did not show this fine structure.

Upon examination of the 3700–3710-cm^{-1} region at 0° (electric vector parallel to the *a*-axis), the remaining intensity appears to have a band maximum at about 3702 cm^{-1}. The band maximum of this feature at 90° was about 3710 cm^{-1}, suggesting that two ν(O–H) bands were present in the 3695–3715-cm^{-1} region, with the lower frequency band showing polarization behavior distinct from that of the 3710-cm^{-1} band. This hypothesis of two closely spaced bands was also reflected by the band analysis for the 3710-cm^{-1} band (Table 3). As the intensity of the higher frequency band at about 3710 cm^{-1} was attenuated, the lower frequency band at 3702 cm^{-1} made a larger contribution to the observed lineshape. This resulted in a shift of the position of this composite band to a lower frequency. A concomitant decrease in the percentage of Lorentzian character of the band and a significant increase in bandwidth were also observed, as the polarization of the electric vector was rotated towards the *a*-axis (Table 3). As the lower frequency band made a proportionally larger contribution to the observed lineshape, the lineshape took on an increasingly greater Gaussian character, which was also indicative of two bands rather than one.

Polarized single-crystal FTIR spectra of dickite in

https://doi.org/10.1346/CCMN.1990.0380602 Published online by Cambridge University Press

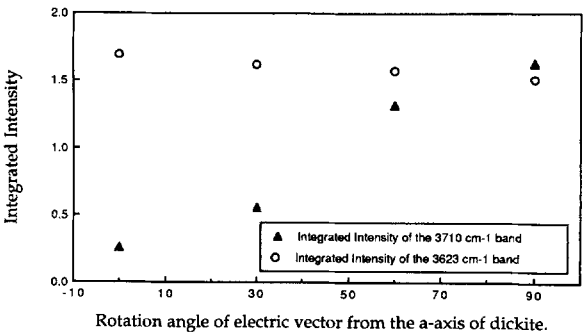

Figure 4. Plot of integrated intensities of the 3623- and 3710-cm^{-1} bands as a function of the angle of polarization of the electric vector with the *a*-axis.

the 700–1300-cm^{-1} region are shown in Figure 5. Upon rotation of the electric vector from the *a*-axis towards the *b*-axis, the 792- and 937-cm^{-1} bands gained intensity, whereas the 911-, 952-, and 1120-cm^{-1} bands lost intensity. The complex lineshape of the 1120-cm^{-1} band indicates the presence of at least two bands, one of which was apparently highly polarized with a transition moment closely aligned to the *a*-axis. The 952-cm^{-1} band was well resolved with polarization of the electric vector parallel to the *a*-axis, but was poorly resolved in the 90° spectrum. Thus, several of the more intense vibrational bands in this region, such as the 1040-cm^{-1} band, were probably optically saturated due to the thickness of the dickite crystals.

Kaolinite

Polarized single-crystal FTIR spectra of Keokuk kaolinite in the ν(O–H) region are shown in Figures 6a and 6b. Similar to the spectra for dickite, the absolute intensity scale is shown for the overlaid spectra (Figure 6a). The position of the ν(O–H) bands at 3620, 3651, 3668, and 3696 cm^{-1} are in good agreement with published IR and Raman spectra of polycrystalline kaolinite (Farmer, 1974; Johnston *et al.*, 1985; Brindley *et al.*, 1986; Prost *et al.*, 1989). The intensities of the 3620- and 3668-cm^{-1} bands were influenced by rotation of the electric vector. An opposite change in intensity occurred for the 3651-cm^{-1} band. Attempts to resolve the spectral components of kaolinite using the non-linear, least-squares program were unsuccessful, due to the lower signal-to-noise ratio obtained for kaolinite in comparison with that for dickite and because kaolinite has four ν(O–H) bands in comparison with only three for dickite.

Low-frequency, polarized single-crystal FTIR spectra of kaolinite are shown in Figure 7. The thickness of the Keokuk kaolinite crystal was less than that of the Ouray dickite crystal; thus, optical saturation was less of a problem for kaolinite. The area of the kaolinite crystals in the *ab*-plane was correspondingly smaller

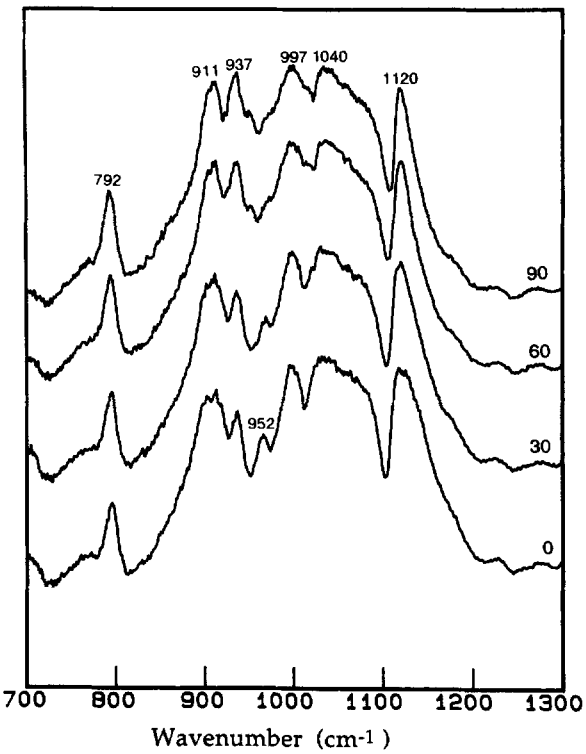

Figure 5. Polarized single-crystal Fourier-transform infrared spectra of Ouray dickite in the 700–1300-cm^{-1} region. Polarization angles listed on right side of figure correspond to angle between electric vector of transmitted IR beam and crystallographic *a*-axis of the dickite crystal.

Table 3. Nonlinear least-squares band analysis of the OH-stretching region of Ouray dickite using a variable Lorentzian-Gaussian fitting function.

Angle (from a)	Frequency	FWHM	Integrated intensity	Lorentzian intensity (%)	Percentage of total area character
Inner OH at 3623 cm^{-1}					
90	3622	11.6	1.52	.69	36.2
60	3622	11.1	1.58	.76	38.1
30	3622	11.8	1.63	.89	46.7
0	3622	12.6	1.70	.95	55.4
Inner-surface OH at 3656 cm^{-1}					
90	3656	12.7	1.03	.99	24.7
60	3656	12.7	1.25	.96	30.1
30	3656	13.3	1.30	.98	37.4
0	3656	13.7	1.11	.97	36.2
Inner-surface OH at 3710–3702 cm^{-1}					
90	3709	21.3	1.63	.71	39.0
60	3709	22.5	1.31	.59	31.8
30	3707	26.6	0.55	.05	15.8
0	3702	28.5	0.26	.05	8.5

FWHM = full-width at half-maximum (cm^{-1}).

https://doi.org/10.1346/CCMN.1990.0380602 Published online by Cambridge University Press

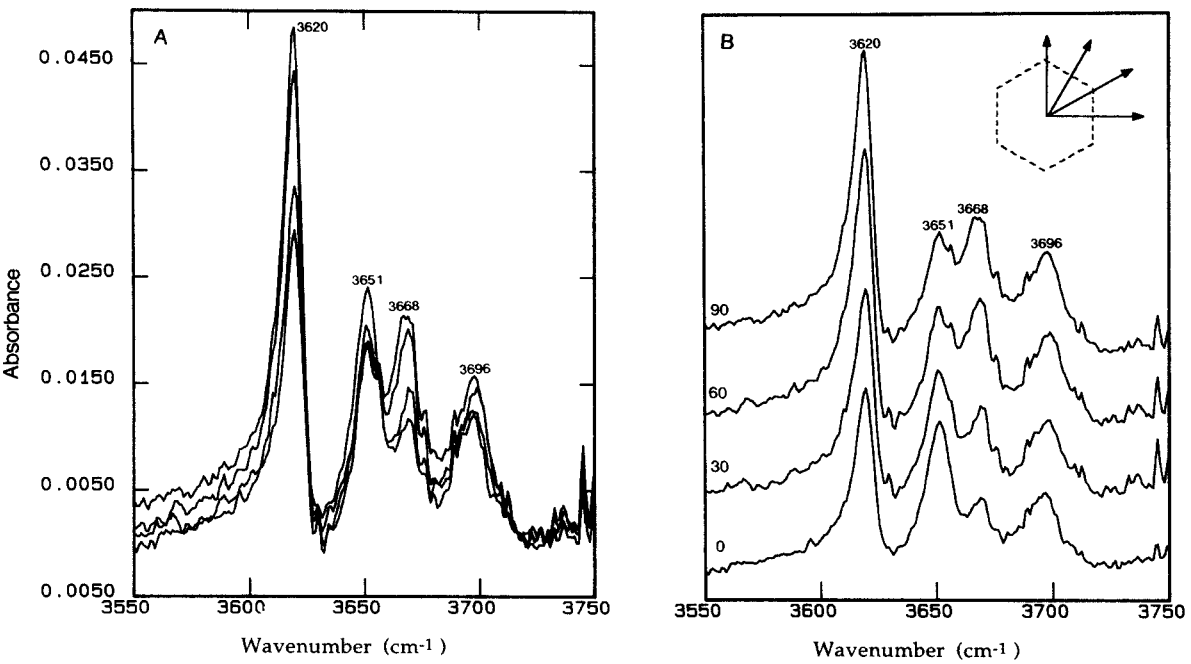

Figure 6. Polarized single-crystal Fourier-transform infrared spectra of Keokuk kaolinite in 3550–3750-cm^{-1} region. (a) Stack plot showing spectra with no y-offset. (b) Same spectra in which listed polarization angles correspond to angle between the electric vector of transmitted IR beam and an arbitrary side of the kaolinite crystal.

than for the dickite crystals. This presented a problem in filling the aperture of the microscope completely with the (001) face of the kaolinite crystal. Upon rotation of the electric vector about the c′-axis, the intensities of the 938-, 1030-, and 1116-cm^{-1} bands changed substantially, whereas the intensity of the 1005-cm^{-1} band decreased. The 794-cm^{-1} band showed some change in lineshape upon rotation of the electric vector around the c′-axis.

DISCUSSION

Hydroxyl-stretching region

The space group of dickite is *Cc*, with the position of the vacant octahedral site in dickite alternating between B and C sites in successive octahedral sheets, as defined by Bailey (1963). This alternating pattern of vacant sites results in the well-known 2-layer structure (c = 14.389 Å) and produces a glide plane, which is absent in kaolinite. For dickite, the symmetry operation of the glide plane is a reflection in the 010 plane followed by translation through half a lattice repeat. This symmetry operation can be seen in the 001 projection of the inner OH groups of dickite, which shows the alternating orientation of the OH groups with respect to the b-axis in successive layers (Figure 8a). Thus, the angle which the OH group makes with the b-axis alternates between positive and negative values similar to that found in the $2M_1$ structure of micas (Vedder and McDonald, 1963).

For space group *Cc*, the dichroic ratio (Turrell, 1972) is given by Eq. (1).

$$D \equiv \frac{I_b}{I_a} = \frac{\dfrac{2\pi\nu C \cos^2\theta}{c\sqrt{\epsilon_b}}}{\dfrac{2\pi\nu C \sin^2\theta}{c\sqrt{\epsilon_a}}} = \left(\frac{\epsilon_a}{\epsilon_b}\right)^{1/2} \cot^2\theta \qquad (1)$$

where θ is defined as the angle between the transition moment of the hydroxyl group and the crystallographic b-axis, c is the speed of light, ϵ is the dielectric constant, C is a constant, and ν is the frequency of light. The 3623-cm^{-1} band has been assigned to the inner hydroxyl OH_i group located between the tetrahedral and octahedral sheets. The experimentally determined dichroic ratio (I_b/I_a) of the inner hydroxyl 3623-cm^{-1} band of dickite is about 0.892, which corresponds to a calculated angle of θ = 47° using Eq. (1). For comparison, the published X-ray and neutron diffraction angles of the orientation of the OH_i group with the b-axis are 25° and 31°, respectively (Table 1).

The intensity of the 3710-cm^{-1} band is strongly attenuated upon rotation of the electric vector away from the b-axis. The experimentally determined dichroic ratio (I_b/I_a) for the 3710-cm^{-1} band is about 6.27, which corresponds to a calculated value of θ = 22°, according to Eq. (1). This angle is clearly within the range of neutron- and X-ray-determined angles listed for the

https://doi.org/10.1346/CCMN.1990.0380602 Published online by Cambridge University Press

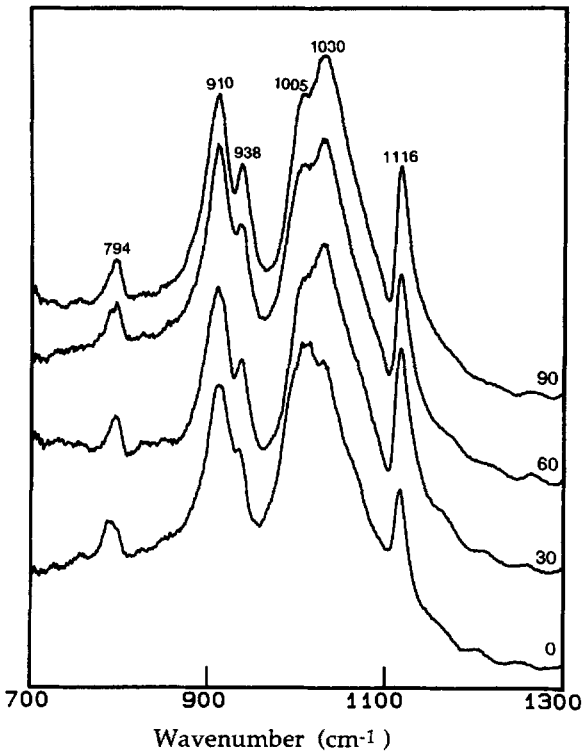

Figure 7. Polarized single-crystal Fourier-transform infrared spectra of Keokuk kaolinite in 700–1300-cm^{-1} region. Polarization angles listed on right side of figure correspond to angle between electric vector of transmitted IR beam and an arbitrary side of the kaolinite crystal.

OH_3 group (Table 1), which range between 5° and 25°. The absorption band at 3710 cm^{-1} appears to have at least two bands which exhibit slightly different polarization behavior. Apparently, the higher frequency component centered at about 3710 cm^{-1} is reduced in intensity to a greater extent than the lower frequency component centered at 3702 cm^{-1} with the electric vector parallel to the *a*-axis. On the basis of the observed polarization behavior, we assign the OH_3 group to the band at 3710 cm^{-1}. Assignment of the lower frequency band at 3702 cm^{-1} is not currently known; however, low-temperature IR studies of dickite have shown clearly that at least two bands are present in this region at 3711 and 3726 cm^{-1} at 5 K (Prost *et al.*, 1987).

The remaining OH-stretching band at 3656 cm^{-1} is herein assigned to the OH_2 and OH_4 groups. Although large variations exist for the neutron and X-ray diffraction positions of the hydrogen atoms of dickite (Table 1), the uncertainties in the positions of the non-hydrogen atoms is much smaller. The average internuclear O···O distances and the Al–O–Al angles for the inner-surface OH groups are presented below:

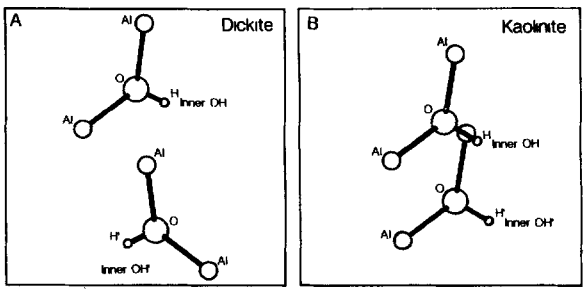

Figure 8. 001 projections of inner OH groups of two layers of (a) dickite and (b) kaolinite.

Group	O···O distance (Å)	Al–O–Al angle
OH_2	2.936	107.5°
OH_3	3.126	104.8°
OH_4	2.955	107.7°

As these data indicate, the non-hydrogen atom distances and angles for the OH_2 and OH_4 groups are similar to each other, which supports their assignment to a common ν(O–H) band. The shorter O···O distances for the OH_2 and OH_4 groups compared with that for the OH_3 group is consistent with their assignment to the lower frequency inner-surface ν(O–H) band (i.e., the 3656-cm^{-1} band). The difference in frequency between 3710 cm^{-1} and 3656 cm^{-1} presumably results from stronger interlayer hydrogen bonding for the latter, as indicated by the smaller internuclear O···O distances.

Neither the position, bandwidth, nor integrated intensity of the 3656-cm^{-1} band was significantly perturbed by rotation of the electric vector around the *c*-axis. Consequently, the calculated angle of the transition moment for OH_2 and OH_4 is 45° ± 5° with respect to the *b*-axis, which compares with neutron and X-ray diffraction angles, which range between 9° and 88°. Although twinning should strongly influence the experimentally determined dichroic ratio by limiting the degree of attenuation, the degree of twinning in dickite was assumed to be small on the basis of the strong extinction of the 3710–3700-cm^{-1} band. Thus, the measured angle of 45° for OH_2 and OH_4 should be reliable to within ±5°. Oriented thin-film IR absorption studies of dickite have shown that the 3656-cm^{-1} band displays the largest increase in intensity upon rotation of the clay film away from normal incidence (Prost *et al.*, 1987). Normal incidence is defined here as an angle of 90° between the direction of the IR beam and the (001) face of the dickite particles. This increase in the out-of-plane$_{(001)}$ intensity indicates that the OH groups responsible for the 3656-cm^{-1} band are oriented nearly parallel to the *c*-axis. This suggested nearly-parallel orientation of the OH_2 and OH_4 groups qualitatively accounts for the smaller-than-expected relative intensity of the 3656-cm^{-1} band compared with the

https://doi.org/10.1346/CCMN.1990.0380602 Published online by Cambridge University Press

3623- and 3710-cm^{-1} bands. The single-crystal IR spectra obtained in this study were collected with the IR beam incident normal to the (001) plane. Thus, vibrational modes which have a transition moment normal to the (001) face, such as the 3656-cm^{-1} band, should have had minimal intensity in this orientation, due to limited overlap between the electric vector of the incident beam and the transition moment of the oscillator.

Kaolinite belongs to the space group C_1 and does not possess the glide plane symmetry element that is present in dickite. As a result, the orientation of the OH groups in kaolinite does not change in successive layers. This fact is illustrated clearly in the 001 projections of kaolinite and dickite shown in Figures 8a and 8b. Thus, complete extinction of all of the OH-stretching bands of kaolinite should have been observed at angles at which the polarization of the electric vector was perpendicular to the transition moment of the particular OH-stretching mode. Complete extinction was not observed for any of the OH-stretching bands, as shown in Figures 6a and 6b. One possible explanation of this observation is the presence of a kaolinite twin. Despite the fact that complete extinction was not achieved, the data are in qualitative agreement with the expected change in polarization behavior predicted by the fact that kaolinite does not possess the glide plane present in dickite. The 3620-cm^{-1} band was considerably more polarized than the inner-OH band at 3623 cm^{-1} of dickite. Greater polarization of the inner OH-stretching band compared with the inner-surface OH groups is also expected for kaolinite, because the angle that this OH group makes with the 001 plane is considerably less than for the inner-surface OH groups (Table 2). As the angle between the OH-transition moment and 001 plane decreases, the overlap between the electric vector of the incident IR beam and the transition moment of the OH group increases, which provides for greater sensitivity to the direction of the incident electric vector.

The intensity of the 3668-cm^{-1} band was also influenced strongly by the direction of the incident electric vector. In comparison, the 3651- and 3696-cm^{-1} bands were not perturbed significantly. There is poor agreement in the literature regarding the positions of the hydrogen atoms of kaolinite (Table 2). Unfortunately, the single-crystal FTIR data presented here for kaolinite do not provide unambiguous information regarding the assignment and orientation of the OH groups. The crystallographic axes of kaolinite could not be determined in this study due to the small size of the kaolinite crystals and the presence of kaolinite twins.

Framework vibrational modes

The 911- and 937-cm^{-1} bands of dickite shown in Figure 5 have been assigned previously as the inner and inner-surface OH-deformation bands (Wada, 1967; Farmer, 1974). The increase in intensity of the 937-cm^{-1} band upon rotation of the electric vector towards the *b*-axis is consistent with the observed increase in intensity of the 3702–3710-cm^{-1} band. Similar to the behavior of the inner OH-stretching band at 3623 cm^{-1}, the corresponding deformation band did not change significantly as a function of polarization. An additional band at 952 cm^{-1}, which is presumably an inner-surface OH-deformation band, appears to be more strongly polarized along the *b*-axis.

For kaolinite, the intensities of the inner and inner-surface OH-deformation bands at 910 and 938 cm^{-1} increased upon rotation of the electric vector from 0° to 90°. The relative intensity change of the 938-cm^{-1} band was greater than that of the 910-cm^{-1} band. These changes correlate directly with the observed frequency increase of the corresponding OH-stretching bands at 3620 and 3668 cm^{-1}. The vibrational band that shows the greatest degree of polarization in the low-frequency spectra of kaolinite, however, was the 1116-cm^{-1} band. Farmer and Russell (1964) assigned this band to a perpendicular Si–O-stretching mode. These data indicate that the horizontal component of the transition moment for this mode is aligned along the *a*-axis. For kaolinite the crystallographic axes could not be unambiguously assigned; thus, the angles listed in Figures 6a, 6b, and 7 are included as a means of comparison of the relative intensity change upon rotation of the electric vector around the c′ axis.

SUMMARY AND CONCLUSIONS

The polarized single-crystal FTIR spectra obtained in this study provide new insight into the location of the OH groups in kaolinite and dickite. For dickite, the orientation of the crystallographic axes was unambiguously determined, and a complete assignment of the observed OH-stretching bands to the four OH groups was established. The position and orientation of the OH groups, determined using the measured dichroic ratios for the ν(O–H) bands, is in reasonable agreement with the available structural data for dickite. The OH-deformation bands were not as well resolved as the ν(O–H) bands; however, the observed changes in the ν(O–H) region were also observed in this region. The thickness of the dickite crystals resulted in slight optical saturation in this region, preventing more quantitative analysis. In comparing the polarization behavior of the ν(O–H) bands of dickite with those of kaolinite, it was necessary to consider the different space groups of these polymorphs. Dickite contains a glide plane, which introduces a left- and right-handed character to the alternating layers. Consequently, the polarization behavior of the ν(O–H) groups was quite distinct from that of kaolinite, in which the glide plane is absent. Unlike dickite, an unambiguous determination of the orientation of the crystallographic axes for kaolinite was not possible due to the smaller size

of the kaolinite crystals and to interferences resulting from probable twinning. The observed polarization data for kaolinite, however, are in qualitative agreement with the change in space group from that of dickite (Cc) to C_1. Given the large uncertainties in the position of the hydrogen atoms present in the published kaolinite and dickite structures, vibrational data should probably be used to constrain the coordinates of the hydroxyl groups in future X-ray and neutron diffraction refinements of dickite.

ACKNOWLEDGMENTS

This work was supported, in part, by the Environmental Sciences Branch of the United States Air Force. The authors thank W. D. Keller for providing the Keokuk kaolinite sample. In addition, we thank W. G. Harris for assistance with the optical mineralogy. Florida Agricultural Experiment Station Journal Series No. R-00710.

REFERENCES

Adams, J. M. (1983) Hydrogen atom positions in kaolinite by neutron profile refinement: *Clays & Clay Minerals* **31,** 352–356.

Adams, J. M. and Hewat, A. W. (1981) Hydrogen atom positions in dickite: *Clays & Clay Minerals* **29,** 316–319.

Bailey, S. W. (1963) Polymorphism of the kaolin minerals: *Amer. Mineral.* **48,** 1196–1209.

Barrios, J., Plançon, A., Cruz, M. I., and Tchoubar, C. (1977) Qualitative and quantitative study of stacking faults in a hydrazine treated kaolinite. Relationship with the infrared spectra: *Clays & Clay Minerals* **25,** 422–429.

Bish, D. L. and Von Dreele, R. B. (1989) Rietveld refinement of non-hydrogen atomic positions in kaolinite: *Clays & Clay Minerals* **37,** 289–296.

Bookin, A. S., Drits, V. A., Plançon, A., and Tchoubar, C. (1989) Stacking faults in kaolin-group minerals in the light of real structural features: *Clays & Clay Minerals* **37,** 297–307.

Brindley, G. W., Kao, C., Harrison, J. L., Lipsicas, M., and Raythatha, R. (1986) Relation between structural disorder and other characteristics of kaolinites and dickites: *Clays & Clay Minerals* **34,** 239–249.

Farmer, V. C. (1974) The layer silicates: in *The Infrared Spectra of Minerals,* V. C. Farmer, ed., Mineralogical Society, London, 331–363.

Farmer, V. C. and Russell, J. D. (1964) The infra-red spectra of layer silicates: *Spectrochimica Acta* **20,** 1149–1173.

Giese, R. F. (1982) Theoretical studies of the kaolin minerals: Electrostatic calculations: *Bull. Mineral.* **105,** 417–424.

Giese, R. F. (1988) Kaolin minerals: Structures and stabilities: in *Hydrous Phyllosilicates (exclusive of Micas),* S.W. Bailey, ed., Reviews in Mineralogy, **19,** Mineralogical Society of America, Washington, D.C., 29–66.

Giese, R. F. and Datta, P. (1973) Hydroxyl orientation in kaolinite, dickite, and nacrite: *Amer. Mineral.* **58,** 471–479.

Johnston, C. T., Sposito, G., Bocian, D. F., and Birge, R. R. (1984) Vibrational spectroscopic study of the interlamellar kaolinite-dimethylsulfoxide complex: *J. Phys. Chem.* **88,** 5959–5964.

Johnston, C. T., Sposito, G., and Birge, R. R. (1985) Raman spectroscopic study of kaolinite in aqueous suspension: *Clays & Clay Minerals* **33,** 483–489.

Johnston, C. T. and Stone, D. A. (1990) Influence of hydrazine on the vibrational modes of kaolinite: *Clays & Clay Minerals* **38,** 121–128.

Joswig, W. and Drits, V. A. (1986) The orientation of the hydroxyl groups of dickite by X-ray diffraction: *N. Jb. Miner. Mh.* 19–22.

Keller, W. D. (1977) Scan electron micrographs of kaolins collected from diverse environments of origin—IV. Georgia kaolin and kaolinizing source rocks: *Clays & Clay Minerals* **25,** 311–345.

Kerr, P. F. (1977) *Optical Mineralogy:* 4th ed., McGraw-Hill, New York 458–459.

Ledoux, R. L. and White, J. L. (1964) Infrared study of selective deuteration of kaolinite and halloysite at room temperature: *Science* **145,** 47–49.

Michaelian, K. H. (1986) The Raman spectrum of kaolinite #9 at 21 deg. C: *Can. J. Chem.* **64,** 285–289.

Prost, R. (1984) Etude par spectroscopie infrarouge a basse temperature des groupes OH de structure de la kaolinite, de la dickite et de la nacrite: *Agronomie* **4,** 403–406.

Prost, R., Dameme, A., Huard, E., and Driard, J. (1987) Infrared study of structural OH in kaolinite, dickite, and nacrite at 300 to 5 K: in *Proc. Int. Clay Conf., Denver, 1985,* L. G. Schultz, H. van Olphen, and F. A. Mumpton, eds., The Clay Minerals Society, Bloomington, Indiana, 17–23.

Prost, R., Dameme, A., Huard, E., Driard, J., and Leydecker, J. P. (1989) Infrared study of structural OH in kaolinite, dickite, nacrite, and poorly crystalline kaolinite at 5 to 600 K: *Clays & Clay Minerals* **37,** 464–468.

Raupach, M., Barron, P. F., and Thompson, J. G. (1987) Nuclear magnetic resonance, infrared, and X-ray powder diffraction study of dimethylsulfoxide and dimethylselenoxide intercalates with kaolinite: *Clays & Clay Minerals* **35,** 208–219.

Rouxhet, P. G., Samudacheata, N., Jacobs, H., and Anton, O. (1977) Attribution of the OH stretching bands of kaolinite: *Clay Miner.* **12,** 171–178.

Sen Gupta, P. K., Schlemper, E. O., Johns, W. D., and Ross, F. (1984) Hydrogen positions in dickite: *Clays & Clay Minerals* **32,** 483–485.

Suitch, P. R. and Young, R. A. (1983) Atom-positions in highly-ordered kaolinite: *Clays & Clay Minerals* **31,** 357–366.

Thompson, J. G., FitzGerald, J. D., and Withers, R. L. (1989) Electron diffraction evidence for C-centering of non-hydrogen atoms in kaolinite. *Clays & Clay Minerals* **37,** 563–565.

Thompson, J. G. and Withers, R. L. (1987) A transmission electron microscopy contribution to the structure of kaolinite: *Clays & Clay Minerals* **35,** 237–239.

Turrell, G. (1972) *Infrared and Raman Spectra of Crystals:* Academic Press, London, 153–158.

Vedder, W. and McDonald, R. S. (1963) Vibrations of the OH ions in muscovite: *J. Chem. Phys.* **38,** 1583–1590.

Wada, K. (1967) A study of hydroxyl groups in kaolin minerals utilizing selective-deuteration and infrared spectroscopy: *Clay Miner.* **7,** 51–61.

Wieckowski, T. and Wiewiora, A. (1976) New approach to the problem of the interlayer bonding in kaolinite: *Clays & Clay Minerals* **24,** 219–223.

Wiewiora, A., Wieckowski, T., and Sokolowska, A. (1979) The Raman spectra of kaolinite sub-group minerals and of pyrophyllite: *Arch. Mineral.* **35,** 5–14.

Young, R. A. and Hewat, A. W. (1988) Verification of the triclinic crystal structure of kaolinite: *Clays & Clay Minerals* **36,** 225–232.

(Received 11 December 1989; accepted 22 May 1990; Ms. 1968)